UCRL-JRNL-230492

Star-Formation in Low Radio Luminosity AGN from the Sloan Digital Sky Survey

W. H. de Vries, J. A. Hodge, R. H. Becker, R. L. White, D. J. Helfand

April 30, 2007

Astronomical Journal

Star-Formation in Low Radio Luminosity AGN from the Sloan Digital Sky Survey

W. H. de Vries, J. A. Hodge, R. H. Becker
University of California, 1 Shields Ave, Davis, CA 95616
IGPP, Lawrence Livermore National Laboratory, L-413, Livermore, CA 94550
devries1@llnl.gov

R. L. White
Space Telescope Science Institute, 3700 San Martin Drive, Baltimore, MD 21218
and

D. J. Helfand
Columbia Astrophysics Laboratory, Columbia University, 550 West 120th Street, New York, NY 10027

ABSTRACT

We investigate faint radio emission from low- to high-luminosity Active Galactic Nuclei (AGN) selected from the Sloan Digital Sky Survey (SDSS). Their radio properties are inferred by co-adding large ensembles of radio image cut-outs from the FIRST survey, as almost all of the sources are individually undetected. We correlate the median radio flux densities against a range of other sample properties, including median values for redshift, [O III] luminosity, emission line ratios, and the strength of the 4000Å break. We detect a strong trend for sources that are actively undergoing star-formation to have excess radio emission beyond the $\sim 10^{28}$ ergs s^{-1} Hz^{-1} level found for sources without any discernible star-formation. Furthermore, this additional radio emission correlates well with the strength of the 4000Å break in the optical spectrum, and may be used to assess the age of the star-forming component. We examine two subsamples, one containing the systems with emission line ratios most like star-forming systems, and one with the sources that have characteristic AGN ratios. This division also separates the mechanism responsible for the radio emission (star-formation vs. AGN). For both cases we find a strong, almost identical, correlation between [O III] and radio luminosity, with the AGN sample extending toward lower, and the star-formation sample toward higher luminosities. A clearer separation between the two subsamples is seen as function of the central velocity dispersion σ of the host galaxy. For systems at similar redshifts and values of σ, the star-formation subsample is brighter than the AGN in the radio by an order of magnitude. This underlines the notion that the radio emission in star-forming systems can dominate the emission associated with the AGN.

Subject headings: galaxies: active — galaxies: starburst — radio continuum: galaxies

1. Introduction

The formation of the bulge component of galaxies and their central black holes is now understood to be tightly linked (e.g., Richstone et al. 1998; Kauffmann & Haehnelt 2000; Heckman et al. 2004). There are several observational lines of evidence for this theoretical claim. For instance, the central velocity dispersion of bulges is found not just to correlate with the mass of the bulge,

but also with the inferred mass of the central black hole (e.g., Ferrarese & Merritt 2000; Gebhardt et al. 2000). Since the correlation between the mass of the central black hole and the bulge exists over a large range of bulge masses, it is thought that, above some lower mass limit, all bulges harbor massive central black holes. Locally, accurate black hole mass measurements have been made for our own Galaxy (e.g., Schödel et al. 2003; Ghez et al. 2005), and the Andromeda galaxy (e.g., Bender et al. 2005). Our own Galactic black hole is rather dormant based on its relatively low X-ray emission (e.g., Baganoff et al. 2003; Xu et al. 2006), but in general these massive black holes are considered a key component of Active Galactic Nuclei (AGN), in which accretion onto the black hole itself can produce large amounts of energy efficiently (e.g., Lynden-Bell 1969; Pringle 1981).

It is of interest, then, to study AGN properties over a large range of luminosities, ranging from the AGN-emission-dominated quasars to galaxies for which the presence of a weak AGN can be inferred through unusual optical emission line ratios. Kauffmann et al. (2003a,b) studied the properties of the host galaxies of AGN, using large, well-defined samples from the Sloan Digital Sky Survey (SDSS, e.g., York et al. 2000; Stoughton et al. 2002). The sheer size of these samples (a few tens of thousands of galaxies) allows for very accurate measurements of sample averages and their trends as function of optical continuum and emission-line (mainly [O III]) luminosities. One of the conclusions from Kauffmann et al. (2003a, hereafter K03a) is that the main difference between low- and high-luminosity AGN is the significant presence of a young stellar population in the latter.

In this paper, we will concentrate on the radio emission properties of a large sample of AGN, similarly selected from the SDSS survey (Data Release 4, Adelman-McCarthy et al. 2006). We use the latest AGN compilation of Kauffmann et al.[1] who used the BPT (Baldwin, Phillips, & Terlevich 1981) diagram of emission line ratios to select for AGN activity. The current version of this catalog contains 80,156 candidate objects which are also covered by the VLA[2] FIRST radio survey (Becker, White, & Helfand 1995). In addition, we selected 14,165 quasars from the DR4 release for which we have FIRST images and [O III] line coverage (limiting the quasar redshifts to < 0.8). These quasars will form the high-luminosity portion of our sample.

We focus our attention on the radio emission of the AGN for several reasons. First, almost all AGN are thought to produce radio flux at some level; even the Galactic black hole, currently in a "quiescent" phase, emits in the radio. Some AGN are extremely luminous in the radio (compared to their optical output) – the so-called radio-loud objects, although we are not considering these specifically, as our average AGN is radio-quiet by a wide margin. Secondly, radio emission is unaffected by intrinsic absorption within each source. It therefore provides a more or less accurate measure of AGN radio output, with the sole caveat being relativistic beaming effects. Since none of our sources are classified as Blazars for which beaming effects can be large, we assume this to play a minor role. Finally, the ready availability of a large-area, high-resolution radio survey in FIRST provides radio information on the large numbers of AGN in its 9033 deg^2 coverage.

There is, however, one apparent problem: almost none of the sources in the SDSS sample are detected by the FIRST survey, with its flux density threshold at 1.4GHz of 1.0 mJy (5σ). Out of 80 154 AGN, only 5 875 (7.3%) are detected directly by the FIRST survey. The relevant numbers for the quasars are only slightly better: 1 493 out of 14 165 (10.5%). Clearly by limiting the sample to the brightest sources, one is ignoring the bulk ($\sim 90\%$) of the population. Fortunately, we can stack radio images, and detect the mean and median peak flux densities of ensembles of undetected sources. This method is discussed in depth by White et al. (2006, hereafter Paper I); we summarize the method in § 2. Given our large sample size, we are able to detect not just the (median) ensemble flux density values, but also discern small trends in those values. For our typical stack sample size of 5000 sources, we attain an rms noise of 2.6μJy, and are therefore very sensitive to small changes in the sample median values as we vary

[1] http://www.mpa-garching.mpg.de/SDSS/DR4

[2] The Very Large Array is an instrument of the National Radio Astronomy Observatory, a facility of the National Science Foundation operated under cooperative agreement by Associated Universities, Inc.

other parameters such as the redshift distribution and the [O III] luminosity distribution. We only have a single sample, so the way we investigate the varying dependencies is by re-grouping the stacks according to the quantity of interest. For instance, if we order the sample by redshift and generate 15 adjacent bins (5343 sources per bin), the resulting radio stacks will be different from the 15 bins sorted by [O III] luminosity; each plot in this paper contains the exact same data, but arranged differently.

The typical median radio flux densities for these sources is found to be on the order of 50 to 100 μJy, well below the FIRST threshold, but clearly within the capabilities of the VLA. Indeed, various very deep, small-scale radio surveys exist (e.g., Hopkins et al. 1998; Richards et al. 1999; de Vries et al. 2002). At these low flux densities, star-formation could account for a large fraction of the radio emission in our objects, since flux density levels of 50 μJy are well within range of starforming galaxies (without AGN) at similar redshifts (see, e.g., Windhorst et al. 1999; Fomalont et al. 2002). We cannot, therefore, assign all of the radio emission to the AGN, as some fraction of the emission may be due to star-formation.

The paper is organized as follows. In § 2 we summarize the stacking method as presented in Paper I. The next section describes the properties of the complete sample of 80,156 sources. We then use emission line ratios as well as the strength of the 4000Å break to isolate two subsamples of 26,715 sources each (§ 3). The first subsample has properties most consistent with the presence of an AGN (the "pure" AGN sample); the second has star-formation characteristics while still meeting the AGN selection criterion of K03a. Section 4 details the differences and similarities of these subsamples, which are discussed in further in § 5.

2. FIRST image Stacking Technique

Paper I demonstrates that it is possible to measure the mean and median radio flux density values of distributions of sources, even though individual sources fall far below the detection threshold of the FIRST survey. Provided that the sample is large enough, one can attain rms noise values in the radio sky well below the canonical FIRST value of 0.15 mJy. Actual snap-shot stacking experiments of blank pieces of sky[3] conform to the expected $1/\sqrt{N}$ behavior in the pixel statistics, down to better than 1μJy. Based on these numbers, it is clear that one can detect stacked point-source mean flux densities of a few tens of μJy with high fidelity.

As outlined in Paper I, we prefer to use the median value of the distributions over the mean. The latter quantity is rather easily affected by outliers with large flux densities (the ones which are actually above the FIRST detection threshold). Simply removing the sources above the threshold from the sample to arrive at the mean of the undetected sources is not robust, as a small change in the cut-off flux density (e.g., from 1.0 to 0.9 mJy) results in a significant change in the mean flux value.

The second concern addressed in Paper I is the calibration of the stacking procedure for effects introduced by the radio data analysis in general and the 'CLEAN' algorithm in particular. Analysis of both stacked artificial sources, and actual sub-threshold sources detected in full-synthesis, deeper radio imaging shows that one does not recover fully the flux that went into the stack. These results are illustrated in Fig. 2 of Paper I; the correction for this "snapshot-bias" for sub-threshold sources is given by $S_{p,corr} = 1.40 S_p$, where S_p is the median peak flux density value. All of our stacked peak flux density measurements have been corrected by this factor.

2.1. Stacking luminosity images

Since most of our subsequent discussion deals with radio luminosities, and not radio flux densities, we have to consider whether there are any distribution peculiarities that might affect these quantities. We do not know the flux density distribution of sub-threshold sources, nor the nature of the sources that make up this population. Below flux densities of a few mJy, the composition of the radio source population changes from AGN-dominated to star-formation dominated (e.g., Windhorst et al. 1999).

There are two ways of calculating the median

[3]No pieces of the sky are truly blank, but will consist of faint, unresolved background objects. Our stacking technique is not sensitive enough to pick up this signal: we measured a background signal consistent with 0μJy to within the 0.9μJy rms noise (for 80 154 empty patches).

radio luminosity. One is simply to stack the cutouts (with pixels in units of Jy), and use the median peak flux density and median redshift (of the sources that were used in the stack) to calculate the median radio luminosity. The tacit assumption here is that those two median values actually describe the same "median object". The alternative approach is to convert each snapshot into a luminosity image using the redshift of the individual source, and then stack these images instead. Each pixel in a snapshot image is converted from flux density to luminosity using the following cosmological parameters: $H_{\rm o} = 70$ km s^{-1} Mpc^{-1}, $\Omega_\Lambda = 0.7$, and $\Omega_{\rm M} = 0.3$.

It turns out that the results are not exactly the same. Table 2 (columns 4 and 5) lists the radio luminosities derived using both methods for the sample sorted in $D_n(4000)$ strength, showing typical differences of less than 25%. For the sake of consistency, we will use the luminosity-stacked values instead of the flux density-stacked ones for the remainder of the paper.

3. Star-formation vs. AGN activity

Our data sample was initially selected based on source locations in the BPT plot (Kauffmann et al. 2003a, see also Kewley et al. 2006). The ratios of the narrow-lines of [N II] and [O III] over the permitted Balmer lines Hα and $H\beta$, respectively, serve as an excellent proxy for the amount of star-formation in an object (e.g., Osterbrock 1989). Our galaxies with AGN cover a large range in the BPT plot, and are thus affected by star-formation to varying degrees; the objects found close to the sample cut-off arc, toward the left of the distribution (see Fig. 1), have optical spectra dominated by emission line ratios commonly associated with ongoing star-formation. It should also be noted that Kauffmann et al. used a more liberal cut for their AGN classification than for instance, Kewley et al. (2001), resulting in a fraction of the sources being more H II region-like than AGN-like. These sources are classified as "composite" in the related Brinchmann et al. (2004) paper.

We use the 4000Å break strength index $D_n(4000)$ as defined by Kauffmann et al. (2003b). This index can be parameterized as the age since the last (instantaneous) episode of star-formation (see Fig. 2 of Kauffmann et al. 2003b), in the sense that smaller break strengths correspond to more recent star-formation[4]. The ranges of the $D_n(4000)$ under consideration for our sources roughly correspond to ages since star-formation between $10^{8.6-10.0}$ years. The short end of this range is comparable to typical galaxy merger timescales (e.g., Springel, Di Matteo, & Hernquist 2005), whereas $\sim 10^{10}$ years at $z \sim 0.2$ is close to the age of the universe and therefore represents the initial burst of star-formation. Since we are not going to distinguish between starbursts of different

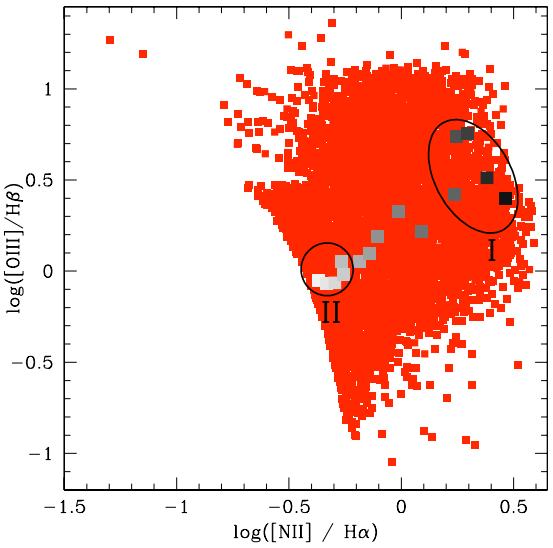

Fig. 1.— Emission line diagnostic plot (BPT, Baldwin, Phillips, & Terlevich 1981) which distinguishes between star-formation-dominated and AGN-dominated systems. The sharp cutoff reflects the selection boundary of Kauffmann et al. (2003a). Points to the left of this cutoff are considered pure star-formation without an AGN contribution. Pure AGN ratios are only expected in the extreme upper right hand corner, so most objects are mixes. The greyscale squares illustrate the progression of low-strength $D_n(4000)$ systems (i.e., most actively star forming) to large break systems (light to dark grey respectively). The circled groups, I and II, are defined in Fig. 2.

[4]It should be noted that Kauffmann et al. (2003a) found that the AGN contribution to the blue continuum, which would give rise to an overestimate of the star-formation rate using this method, is small enough to be ignored for these objects.

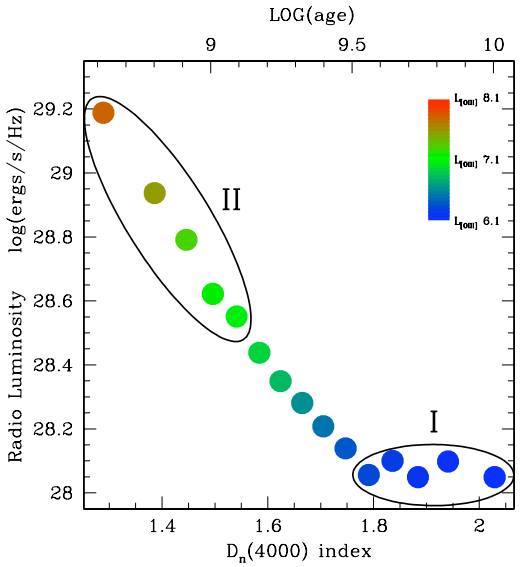

Fig. 2.— Radio Luminosity as function of $D_n(4000)$ strength. The bins, each containing about 5000 sources, are sorted in order of increasing $D_n(4000)$ strength (from left to right), and are coded for [O III] luminosity. The D_n index is not very dependent on redshift; the median redshifts range from 0.12 down to 0.07 (from left to right in the plot). The age indicated on the top of the plot is the inferred age since the last burst of star-formation (in years), based on a linear conversion between $D_n(4000)$ and age (see text). The subsamples marked I and II are described in the text.

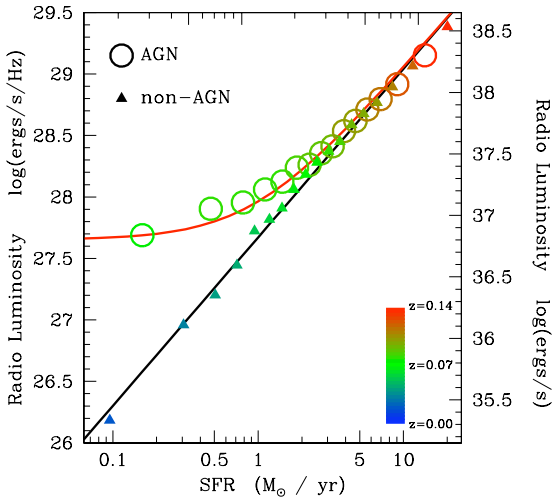

Fig. 3.— Correlation between fiber aperture-corrected star-formation rate, based on the strength of the $D_n(4000)$ break (Brinchmann et al. 2004), and the radio luminosity. The circles represent our sample, and the small triangles are star-forming galaxies without an AGN (taken from Brinchmann et al.). The least-squares fit to the non-AGN data points (black line) is given by: $\log(L_R^{\rm non-AGN}) = (1.37\pm0.02)\log({\rm SFR}) + (27.67\pm 0.01)$. The red line represents the sum of the non-AGN component $L_R^{\rm non-AGN}$ and a constant 4.5×10^{27} ergs s^{-1} Hz^{-1} due to the AGN.

metallicities, we are approximating the relation between age and $D_n(4000)$ by a straight line over the $D_n(4000)$ range 1.3 to 2.0 (the relevant range for our sample): $\log({\rm age}) = 6.21 + 1.87\, D_n(4000)$, with age given in years.

The results for median radio luminosity as function of the strength of the 4000Å break are plotted in Fig. 2. It is clear that the brightest radio emission is associated with the smallest breaks (i.e., the most recent episodes of star-formation). The approximate time since the last epoch of star-formation is given across the top of the plot. Above a $D_n(4000)$ index of about 1.8, there is no change in radio luminosity, which levels off at about 10^{28} ergs s^{-1} Hz^{-1}. This might reflect the absence of any contribution to the radio emission from star-formation. The color coding indicates the [O III] luminosity, which is also seen to decline steeply as $D_n(4000)$ increases.

3.1. Line emission diagnostics

As a double check on the level of star-formation, we can see where the $D_n(4000)$-sorted data points from Fig. 2 land on the BPT plot. In other words, do the sources with the low $D_n(4000)$ values have emission line ratios that reflect a higher incidence of star-formation? The results are plotted in Fig. 1 as a grayscale sequence of squares, running from light-gray to black for the small-to-large valued $D_n(4000)$ systems. It is clear that these two quantities do correlate rather well for our objects, and trace out a sequence of decreasing star-formation versus increasing 4000Å break strength. The gray squares in the top right corner have emission line

ratios completely consistent with pure AGN emission, whereas the squares to the left are significantly affected by star-formation.

The combination of Figs. 1 and 2 leads us to suggest that for the "pure" AGN cases as indicated by large 4000Å breaks, the radio luminosity is strictly due to the AGN with average luminosities near 10^{28} ergs s^{-1} Hz^{-1}. The additional radio luminosity we see for other sources can be attributed completely to ongoing star-formation. This star-forming component can be an order of magnitude more luminous than the radio component due to the AGN.

Brinchmann et al. (2004) use the strength of the 4000Å break to calculate the inferred star-formation rate (their sample not only encompasses our AGN sample, but also non-AGN which land to the left of the distribution in Fig. 1). They corrected for the limited angular extent of the SDSS fiber which typically does not contain all of the light of the galaxy. We use these corrected values to sort our sample in ascending order of star-formation rate. The median stacked radio luminosities for 15 bins of ~ 5000 sources each are calculated and plotted against median star-formation rate in Fig. 3. The strong correlation again underlines the importance of the star-formation component to the overall radio luminosity, even for systems containing AGN. The 10^{28} ergs s^{-1} Hz^{-1} "ground-state" radio luminosity from Fig. 2 corresponds, based on this plot, to a star-formation rate of ~ 1 M$_\odot$ yr^{-1}, or less, whereas the largest radio luminosities from Fig. 2 have rates exceeding 10 M$_\odot$ yr^{-1}.

The non-AGN portion of the Brinchmann et al. sample, once sorted by star-formation rate, exhibit a very tight correlation with median radio luminosity (Fig. 3). The least squares fit is given by $\log(L_{\rm R}^{\rm non-AGN}) = (1.37\pm0.02)\log(\rm SFR)+(27.67\pm 0.01)$. This slope of 1.37 is almost identical to that of Bell (2003) who find a slope of 1.30 for radio luminosities less than 6.4×10^{28} ergs s^{-1} Hz^{-1}. The Bell results, however, show a different normalization, suggesting they underestimate the amount of star-formation for a given radio luminosity by a factor of 2.

Even more remarkable than the tight correlation between estimated star-formation rate and mean radio luminosity over two orders of magnitude is that the AGN contribution to the radio luminosity can be represented by a constant (4.5×10^{27} ergs s^{-1} Hz^{-1}) which, once added to the star-formation estimate (black line), gives us the red line. This single constant implies that the AGN output (in the radio) is more or less independent of the star-formation level of the host galaxy. It is also a better measure of this AGN "ground-state" than the 10^{28} value derived from Fig. 2.

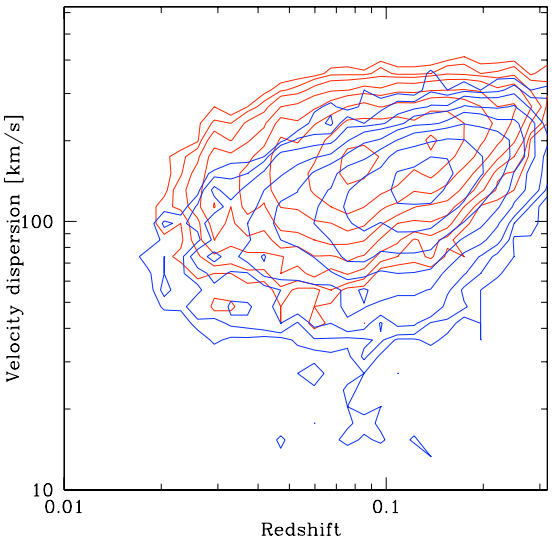

Fig. 4.— Distribution densities for the 5 lowest (red) and 5 highest (blue) radio luminosity bins of Fig. 2. While the redshift coverage is comparable, there is a clear dependency on the strength of the $D_n(4000)$ index in the sense that it is easier for a given burst of star-formation to "fill in" the 4000Å break in a smaller, low σ system. The density contours are given by 2^n, with $n = 2, 3, 4, \cdots$.

In summary, since the star-formation rates are based on the $D_n(4000)$ values, we will use the latter to isolate two subsamples; one that presumably has no, or very little, ongoing star-formation (labeled I in Figs. 1 and 2), and one that contains the systems with the most ongoing star-formation (labeled II). Each one of these subsamples contain 26,715 sources.

4. A closer look at the "pure" AGN subsample

We designate the five rightmost data points in Figs 1 and 2 as representing the most AGN-like

sources. Their emission line ratios are the least star-formation-like, and their median [O III] and [O II] luminosities are among the lowest in our sample (see Table 2).

Figure 4 shows the distribution densities in redshift versus velocity dispersion space for the large 4000Å break, low star-formation sources (red contours), compared to the sources with the smallest 4000Å break and the highest levels of star-formation (blue contours). The redshift distribution for each subset is comparable, whereas there is a clear offset in velocity dispersion. This is most likely due to the way the subsets have been selected. For a given burst of star-formation with some upper limit to its optical luminosity, it will appear more prominent (with a consequently lower value of the $D_n(4000)$ index) in smaller galaxies than in large systems. Since the mass and size of the galaxy spheroid scales with its central velocity dispersion (e.g., Gebhardt et al. 2000; Ferrarese & Merritt 2000), we will be biased toward finding more star-formation among the lower σ systems.

4.1. Radio Luminosity and redshift dependence

Luminosity, as in all flux-limited samples, is closely correlated with redshift, resulting in an apparent correlation that is dominated by the lack of bright sources locally, and faint sources at higher redshifts (due to the detection limit). This is illustrated in Fig. 5. Both subsamples I and II were sorted in redshift, and divided up into 13 bins of 2056 sources each. The "pure" AGN-like bins are plotted as pentagons, and the sources most affected by star-formation as stars. In addition, we plotted 7 bins of 2025 quasars each, depicted as green squares.

It is immediately clear that the median radio luminosities of the quasars are directly comparable to the narrow-line AGN values. There is no a-priori reason for the quasar radio luminosity medians not to be much brighter than the galaxies, but their values are comparable at the same redshift. The quasar radio luminosities are slightly less than the star-formation values, and slightly more than the AGN subsample values (at the same redshift). On the other hand, quasars *are* consistently brighter in [O III] luminosity than the narrow-line AGN at similar redshifts (see Fig. 6).

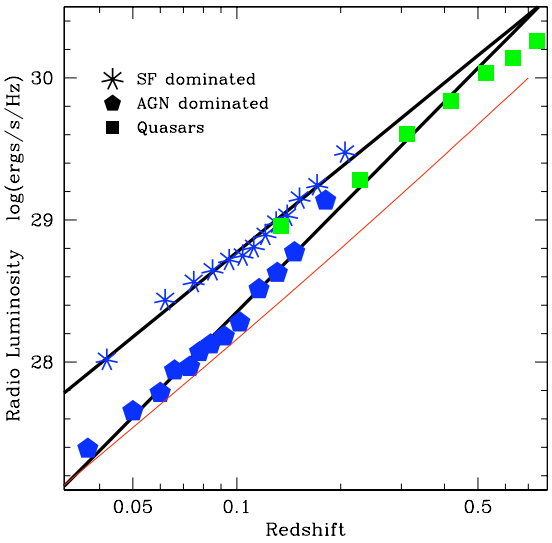

Fig. 5.— Radio luminosity as function of redshift. The narrow-line AGN sample is separated into AGN dominated (I, pentagons) and star-formation dominated (II, stars) parts. In addition, 7 low-redshift quasar bins (squares) are overplotted. The least squares fits are: $\log(L_R) = (1.98\pm0.07)\log(z)+(30.75\pm0.07)$, and $\log(L_R) = (2.45\pm0.11)\log(z)+(30.81\pm0.12)$ for subsamples I and II respectively. The red solid line indicates the radio luminosity of a constant 60 μJy source.

The fact that the median radio luminosity is the same would suggest that we are observing an isotropic emission component, and not orientation / obscuration-dependent quantities like emission lines and the presence of broad permitted lines. The median radio luminosity therefore underlines the validity of the standard AGN unification model (e.g., Barthel 1989; Antonucci 1993).

Another result based on Fig. 5 is that the star-formation-dominated galaxies are brighter in the radio than the pure AGN galaxies, albeit that the difference becomes smaller at redshifts beyond 0.1 (where both samples I and II merge into the low end of the quasar trend). The more or less constant offset of a factor ~ 3 (0.5 in log) between the two subsamples (below $z \sim 0.1$) suggests that the average radio luminosity due to the AGN accounts for at most 25% of the total radio emission during an ongoing phase of star-formation.

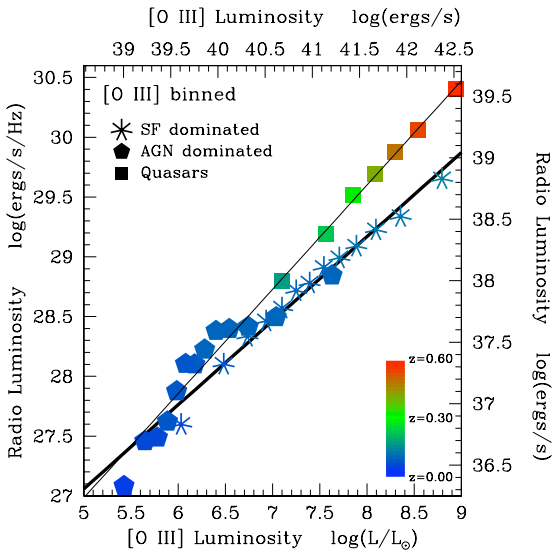

Fig. 6.— Correlation of median values for radio luminosity and [O III] luminosity. The color indicates the median redshift for a particular bin. The 7 squares are broad-line AGN / Quasars. The units on the top and right hand side are converted from the measured values by the following constants: $\log(1.4 \times 10^9)$ Hz, and $\log(3.826 \times 10^{33})$ ergs/s for the x-axis (observing frequency) and y-axis (bolometric luminosity Sun) respectively. Note that for all these points the radio luminosity is at least 3 orders of magnitude lower than typical radio-loud objects. Symbols are the same as in Fig. 5.

4.2. [O III] luminosity as AGN activity indicator

The [O III] emission-line luminosity offers another way of gauging the AGN output. Kauffmann et al. (2003a) estimate that perhaps as little as 7% of the [O III] line emission can be attributed to star-formation in their AGN composite spectrum. This means that, even though both the radio and [O III] luminosities depend on redshift, their correlation should be relatively free of redshift bias (by dropping out of the ratio).

For this purpose, we first order the sample in [O III] luminosity, and then stack the cutouts to calculate the median radio luminosity. The [O III] luminosities have been corrected for extinction using the Hα / Hβ emission line ratio, under the assumption that the [O III] emission is co-spatial (see K03a). The [O III] sorting and stacking also helps in minimizing the redshift differences among the bins. Ideally, one would like to have similar source redshift distributions for each [O III] luminosity bin, which would in effect isolate one from the other.

The results are presented in Fig. 6. We see a strong correlation between [O III] and radio luminosity. For comparison, we also included seven bins of low-redshift quasars. The spectral coverage of the SDSS is such that the [O III] emission line is included in the spectrum up to redshifts of ~ 0.8. This results in a sample of 14,165 DR4 quasars that have $z < 0.8$ and are covered by the FIRST survey. We split the sample into seven equal-sized bins, sorted in [O III] luminosity. Since we are looking at presumably unobscured quasars, we do *not* correct the [O III] luminosities for intrinsic extinction[5].

The two solid lines are least squares fits to the quasars and the star-formation subsample. The first ten data points of the AGN subsample (pentagons) are more or less consistent with the quasar relation, though we do note that there are excursions along the quasar fit. This may have to do with the extinction correction being less than ideal for the AGN subsample. The star-formation subsample does not exhibit similar behavior. The fits are:

$$L_{r,\mathrm{AGN}} = (0.87 \pm 0.02) L_{[\mathrm{OIII}]} + (2.5 \pm 0.8)$$
$$L_{r,\mathrm{SF}} = (0.70 \pm 0.03) L_{[\mathrm{OIII}]} + (9.1 \pm 1.2) \quad (1)$$

with all the luminosities in units of log(ergs/s). It should be noted that the origin of the radio emission is different for the two subsamples. For the AGN- dominated sample the radio emission is largely due to the AGN (though the star-formation component dominates at the highest luminosities, see Fig. 3), whereas the AGN component is only a

[5] We know that the main sample of galaxies has to have some extinction towards the AGN (they would otherwise appear as type 1 Seyfert objects), so correcting for the [O III] luminosity (mainly due to the AGN) makes sense. But since the quasars *are* type 1 objects, we will assume that the corrections for the quasars are considerably smaller than the typical factor ~ 10 corrections in the median [O III] luminosity for the galaxies.

small contributor for the star-formation subsample. As such, it is clear that the differences in the [O III] – radio luminosity relations cannot be explained by a simple translation along either the [O III] or the radio luminosity axes. From Fig. 5 we already know that the starforming subsample is brighter in the radio than either the AGN or quasar samples (at the same redshifts). Therefore, the correct conclusions from Fig. 6 are: the star-forming subsample is both brighter in [O III] *and* in radio luminosity than the AGN subsample at the same redshift, and they have a different slope. Also, the AGN subsample has a similar slope to the quasar sample, which is what one would expect if the AGN are obscured quasars.

4.3. Velocity Dispersion

The central velocity dispersions of galaxies have been found to correlate tightly with the inferred masses of their central black holes (e.g., Ferrarese & Merritt 2000; Gebhardt et al. 2000). The latter quantity also scales with the mass of the stellar bulge. There is some evidence that the most massive bulge systems are more likely to be radio loud compared to less massive systems (e.g., Laor 2000; Lacy et al. 2001), but in our cases we derive median radio luminosities well below what one would consider radio-loud objects. As such, our analysis pertains more to ordinary systems covering a range of AGN indicators (see § 3).

The results are shown in Fig. 7. It is clear that there is a trend for the most massive systems (highest values of σ) to have the highest radio luminosities. This should not come as a surprise, based on the correlations between black hole mass and bulge mass. As seen in § 4.1, the median radio luminosity is apparently not very much affected by orientation effects (since the radio luminosities are comparable for quasars and AGN to within a factor of two at the same redshift), and provides a rather clean measure of the AGN output (at least for the "pure" AGN subsample). This then would presumably scale nicely with the mass of the central black hole, giving rise to the tight correlation between median radio luminosity and velocity dispersion (see Fig. 7, pentagon symbols). The least-squares fit to the star-formation subsample (star-shaped symbols) is given by:

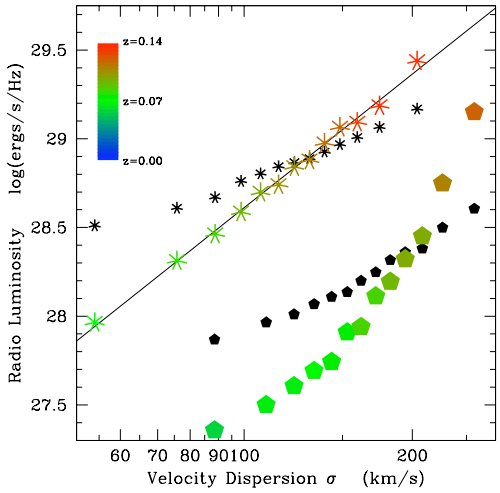

Fig. 7.— Median radio luminosity as function of central velocity dispersion σ of the host galaxy, for the AGN dominated (I, pentagons) and star-formation dominated (II, stars) subsamples. The spread in median redshift is indicated by the color coding. The close correlation between the median values of the velocity dispersion and the radio luminosity is apparent, especially for the star-formation sample. The small symbols indicate where the colored dots would lie if we use its median redshift and the redshift – radio luminosity correlation of Fig. 5. Note that the offsets are along the y-axis. Low σ galaxies are underluminous in the radio compared to the average redshift trend, and the most massive galaxies are overluminous in the radio (this holds true for both subsamples).

$$L_{r,\mathrm{SF}} = (2.50 \pm 0.05) \log(\sigma) + (23.61 \pm 0.10). \quad (2)$$

The AGN-dominated sample does not allow for a straight line (in log-log) fit, which may indicate other dependencies beyond a simple velocity dispersion / galaxy mass scaling.

One thing we need to check though, is the effect the small range in redshift may have on radio luminosity. Based on their tight correlation in Fig. 5, a small change in median redshift may account for most of the trend we see in Fig. 7. To this end, we calculate the median redshift of the sources used for each velocity dispersion bin, and applied the

redshift – radio luminosity fits from Fig. 5 to infer the radio luminosity that way. These values are overplotted as the smaller black symbols (so each σ bin has two radio luminosities associated with it). Now, if the large and small symbols would closely track each other, then the correlation between velocity dispersion and radio luminosity is spurious due the sample being flux-limited. However, since this is not the case, the radio luminosity – velocity dispersion correlation is real.

Note that the offset in radio luminosity between the star-formation dominated and "pure" AGN subsamples is even larger than in Fig. 5, at about an order of magnitude compared to a factor of about 3 (for $z < 0.1$). Clearly for some objects at similar redshifts and similar mass (velocity dispersion), star-formation can account for 90% of the total radio luminosity. This would also suggest that the correlation for the star-formation subsample is driven by the bulge mass – σ relation (higher σ equals a more massive galaxy, which translates into a higher absolute amount of star-formation for a given $D_n(4000)$ value). The radio luminosity for the "pure" AGN subsample (pentagons in Fig. 7) on the other hand, scales with the mass of the central black hole, which itself scales with the bulge mass (which is directly related to the velocity dispersion).

5. Discussion and Summary

We note the correlations of the median values of the [O III] and radio luminosities in § 4.2 and Fig. 6, in particular the similar ratios for the AGN, star-formation, and quasar subsamples. Given that the mechanisms responsible for the radio emission are thought to be different between the AGN and star-formation subsamples, this comes as a surprise. Our work is not the first that that touches on this subject. For instance, Wills et al. (2004) worked on a sample of nearby ($z < 0.05$), low-luminosity AGN taken from a 2Jy radio sample. They found an [O III] – radio luminosity slope of 0.85, based on a sample of a few dozen sources[6]. This value is comparable to the AGN value (0.87, see Eqn. 1), but that may be coincidental since their sample is so much brighter than ours (compare the solid line in Fig. 8 to our median values);

[6]We converted their 5GHz radio flux densities to 1.4GHz values using a constant spectral radio index of −0.5

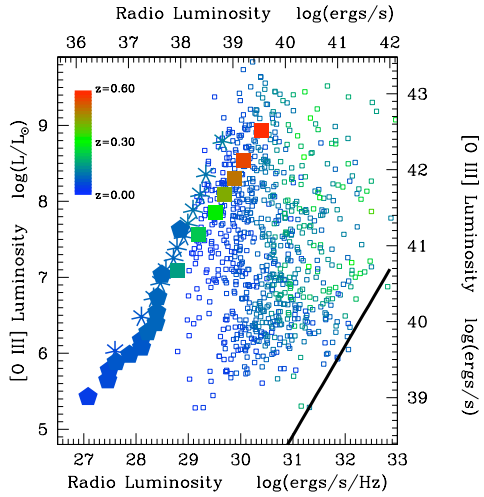

Fig. 8.— Comparison of the correlation between [O III] and radio luminosities (see Fig. 6, note that the axes are switched) to values from the literature. The sample of Best et al. (2005) contains SDSS objects with a radio flux of > 5mJy and are represented by the small open squares (color coded with redshift). The offsets in radio luminosity between our median values and theirs can exceed 3 orders of magnitude. It should be noted that our sample of 80,156 includes the Best et al. sample, underlining the severe bias one introduces by selecting the brightest radio sources. The solid line is the fit from Wills et al. (2004) on local low-luminosity AGN.

even though the Wills et al. sample is considered low radio luminosity, it is still more than 3 orders of magnitude brighter than our median values. They are probing the brightest part of the radio source population. This can be put into more perspective by comparing our sample to the one of Best et al. (2005). Their paper is also based on FIRST and SDSS data. Actually, their data-set is wholly contained within ours.

In Fig. 8, we replot the data from Fig. 6 onto the data from Best et al. We only include sources from their sample (open square symbols) that are both in our sample and have detected [O III] emission (Fig. 9, lower right panel from Best et al. includes a set of [O III] non-detections). Our median [O III] values cover the exact same range as the Best et al. sample; the main difference is the radio luminosity.

Since our data represent median values, it implies that a full 50% of the sources are located to the *left* of our data-points. The fact that the Best et al. data can be up to more than 3 orders of magnitude brighter (in the radio) illustrates the severe radio selection bias of their sample. It also makes it clear that one has to be careful in interpreting possible correlations between [O III] and radio luminosities. The Best et al. sample would result in a much steeper relation.

Since our sample has not been selected on radio properties, and since we include *all* sources in the median calculations, we consider our median [O III] – radio luminosity correlation more robust than previous work based on radio-selected samples[7]. Consequently, one can use the median radio luminosity for the star-formation subsample to estimate the star-formation rate. Hopkins et al. (2003) compares various star-formation indicators using SDSS data, and incorporates the radio-derived star-formation rate method of Bell (2003). The inferred star-formation rates are listed in Table 3, and range from less than 1 to about 20 $M_\odot$ per year. These modest star-formation rates are consistent with values derived through, for instance, Hα luminosities of star-forming galaxies that have been detected by FIRST (Hopkins et al. 2003). The listed values should not be taken at face value, however. On the one hand there is an unknown AGN contribution to the overall radio luminosity which inflates the star-formation rate, and on the other hand our median stacking technique is insensitive to extended (beyond ~ 6 arcseconds) radio emission, causing it to underestimate the actual radio luminosity and star-formation rate.

In fact, we measure slightly different sizes for the AGN and star-formation subsamples: $5.9'' \pm 0.3''$ by $6.4'' \pm 0.4''$ and $5.2'' \pm 0.2''$ by $5.7'' \pm 0.2''$, respectively. The AGN sizes are comparable to the median size for SDSS quasars of $6.4''$ by $7.0''$ (also along RA and DEC), as given in Paper I. This implies that there is no extended radio emission detected for the star-formation subsample, while some has been detected for the AGN subsample beyond the $\sim 5.4''$ FWHM of the FIRST point-spread-function.

[7]That is not to say that our sample is without biases: galaxies in our sample have to have measurable emission-line ratios.

5.1. Summary

Combining a large number of objects across a range of AGN activity from the SDSS with the FIRST radio survey allows us to correlate various sample statistics with radio emission at levels that are too low for individual sources to be detected. We are able to measure median radio emission down to a few tens of μJy, well below the FIRST detection threshold.

We find the following quantities to correlate strongly with the median radio luminosity:

1. $D_n(4000)$ index / star-formation rate. This index traces the amount of star-formation in a given galaxy by measuring the amount of blue light relative to the red. Low values of the $D_n(4000)$ index correspond to more active star-formation, and are found to have the highest median radio luminosities (more than an order of magnitude larger than high-index objects).

2. [O III] luminosity. Higher levels of [O III] luminosity correspond to higher median radio luminosities. This is true over at least 3 orders of magnitude. The [O III] – radio luminosity correlation for the "pure-AGN" subsample is consistent with the same relation for quasars, but extended towards lower luminosities. The highest levels of [O III] and median radio emission are seen among the "pure-star-formation" subsample, with levels comparable to the quasar ones.

3. Central velocity dispersion σ. Generally, higher values of σ (i.e., larger galaxies) correspond to larger median radio luminosities. However, there are clear differences between the AGN and star-formation dominated subsamples. For a given median radio luminosity, star-forming systems have a much smaller σ than AGN-dominated systems. Conversely, for a given galaxy size and σ, star-formation dominated systems can be an order of magnitude more luminous in the radio than the AGN-dominated systems.

We furthermore find that the AGN contribution to the overall median radio luminosity is roughly

constant in these galaxies at the 5×10^{27} ergs s^{-1} Hz^{-1} level. The other component is very tightly correlated to the star-formation rate (as derived from the optical spectrum). This also implies that if one is considering a system without an AGN, its star-formation rate can be accurately assessed using the radio luminosity of the system. There is no indication that this correlation cannot be extended to star-formation rates below 0.1 $M_\odot$ / yr.

It is clear that by studying (median) statistical properties of carefully selected and representative samples, one can infer subtle trends that otherwise are either too small to detect, or are masked by source intrinsic variations. Our median radio luminosity measurements are at least a few orders of magnitude below typical studies (see Fig. 8), and provide a much less-biased view of the radio properties of galaxies. Methods such as that used in this paper hold great potential when applied to future, large-scale multi-wavelength surveys.

We like to thank the anonymous referee for helpful comments. The work by WDV and RHB was partly performed under the auspices of the U.S. Department of Energy, National Nuclear Security Administration by the University of California, Lawrence Livermore National Laboratory under contract No. W-7405-Eng-48. JAH acknowledges support of the GAANN Fellowship from the U.S. department of Education. The authors also acknowledge support from the National Radio Astronomy Observatory, the National Science Foundations (grant AST 00-98355), and the Space Telescope Science Institute.

REFERENCES

Adelman-McCarthy, J. K., Agüeros, M. A., Allam, S. S., et al. 2006, ApJS, 162, 38

Antonucci, R. 1993, ARA&A, 31, 473

Baganoff, F. K., Maeda, Y., Morris, M., et al. 2003, ApJ, 591, 891

Baldwin, J. A., Phillips, M. M., & Terlevich, R. 1981, PASP, 93, 5

Barthel, P. D. 1989, ApJ, 336, 606

Becker, R. H., White, R. L., & Helfand, D. J. 1995, ApJ, 450, 559

Bell, E. F. 2003, ApJ, 586, 794

Bender, R., Kormendy, J., Bower, G., et al. 2005, ApJ, 631, 280

Best, P. N., Kauffmann, G., Heckman, T. M., & Ivezić, Ž. 2005, MNRAS, 362, 9

Brinchmann, J., Charlot, S., White, S. D. M., Tremonti, C., Kauffmann, G., Heckman, T., & Brinkmann, J. 2004, MNRAS, 351, 1151

de Vries, W. H., Morganti, R., Röttgering, H. J. A., Vermeulen, R., van Breugel, W., Rengelink, R., & Jarvis, M. J. 2002, AJ, 123, 1784

Ferrarese, L, & Merritt, D. 2000, ApJ, 539, L9

Fomalont, E. B., Kellermann, K. I., Partridge, R. B., Windhorst, R. A., Richards, E. A. 2002, AJ, 123, 2402

Gebhardt, K., Bender, R., Bower, G., et al. 2000, ApJ, 539, L13

Ghez, A. M., Salim, S., Hornstein, S. D., Tanner, A., Lu, J. R., Morris, M., Becklin, E. E., & Duchêne, G. 2005, ApJ, 620, 744

Heckman, T. M., Kauffmann, G., Brinchmann, J., Charlot, S., Tremonti, C., & White, S. D. M. 2004, ApJ, 613, 109

Hopkins, A. M., Mobasher, B., Cram, L., & Rowan-Robinson, M. 1998, MNRAS, 296, 839

Hopkins, A. M., Miller, C. J., Nichol, R. C., Connolly, A. J., Bernardi, M., Gómez, P. L., Goto, T., Tremonti, C. A., Brinkmann, J., Ivezić, Ž., & Lamb, D. Q. 2003, ApJ, 599, 971

Kauffmann, G., & Haehnelt, M. 2000, MNRAS, 311, 576

Kauffmann, G., Heckman, T. M., Tremonti, C., Brinchmann, J., et al. 2003a, MNRAS, 346, 1055

Kauffmann, G., Heckman, T. M., White, S. D., et al. 2003b, MNRAS, 341, 33

Kewley, L. J., Dopita, M. A., Sutherland, R. S., Heisler, C. A., &Trevena, J. 2001, ApJ, 556, 121

Kewley, L. J., Groves, B., Kauffmann, G., & Heckman, T. 2006, MNRAS, in press (astro-ph/0605681)

Lacy, M., Laurent-Muehleisen, S. A., Ridgway, S. E., Becker, R. H., White, R. L. 2001, ApJ, 551, L17

Laor, A. 2000, ApJ, 543, L111

Lynden-Bell, D. 1969, Nature, 223, 690

Magorrian, J., Tremaine, S., Richstone, D., et al. 1998, AJ, 115, 2285

Osterbrock, D. E. 1989, "Astrophysics of Gaseous Nebulae and Active Galactic Nuclei", University Science Books

Pringle, J. E. 1981, ARA&A, 19, 137

Richards, E. A., Fomalont, E. B., Kellermann, K. I., Windhorst, R. A., Partridge, R. B., Cowie, L. L., & Barger, A. J. 1999, ApJ, 526, L73

Richards, G. T., Hall, P. B., Vanden Berk, D. E., et al. 2003, AJ, 126, 1131

Richstone, D., Ajhar, E. A., Bender, R. et al. 1998, Nature, 395, 14

Schödel, R., Ott, T., Genzel, R., Eckart, A., Mouawad, N., & Alexander, T. 2003, ApJ, 596, 1015

Schneider, D. P., Fan, X., Hall, P. B., et al. 2003, AJ, 126, 2579

Springel, V., Di Matteo, T., & Hernquist, L. 2005, MNRAS, 361, 776

Stoughton, C., Lupton, R. H., Bernardi, M., et al. 2002, AJ, 123, 485

White, R. L., Helfand, D. J., Becker, R. H., Glikman, E., & de Vries, W. 2006, ApJ, in press (Paper I)

Windhorst, R. A., Hopkins, A., Richards, E. A., & Waddington, I. 1999, in "The Hy Redshift Universe", ASP Conference Series, Vol 193, eds. A. J. Bunker & W. J. M. van Breugel, p. 55

Wills, K. A., Morganti, R., Tadhunter, C. N., Robinson, T. G., & Villar-Martin, M. 2004, MNRAS, 347, 771

Xu, Y.-D., Narayan, R., Quataert, E., Yuan, F., & Baganoff, F. K. 2006, ApJ, 640, 319

York, D. G., Adelman, J., & Anderson, Jr., J. E., et al. 2000, AJ, 120, 1579

This 2-column preprint was prepared with the AAS LaTeX macros v5.2.

TABLE 1
MEDIAN RESULTS FOR STAR-FORMATION BINNING

$z_{\rm median}$	SFR [$M_\odot$ / yr]	$\log(L_{\rm radio})$ [ergs/s/Hz]	$F_{\rm peak}$ [μJy]	$D_n(4000)$
0.0784	0.15	27.69±0.02	61.7±3.6	1.814
0.0845	0.47	27.90±0.02	80.4±3.6	1.754
0.0819	0.79	27.96±0.02	91.0±3.8	1.728
0.0832	1.12	28.06±0.01	101.8±3.9	1.704
0.0842	1.47	28.14±0.01	114.2±3.4	1.697
0.0865	1.85	28.24±0.01	128.0±3.2	1.683
0.0908	2.26	28.26±0.01	127.1±3.8	1.671
0.0946	2.72	28.36±0.01	139.3±3.6	1.653
0.0994	3.26	28.41±0.01	143.9±3.5	1.639
0.1045	3.90	28.54±0.01	172.9±3.6	1.625
0.1081	4.68	28.62±0.01	190.7±3.8	1.612
0.1151	5.65	28.71±0.01	193.5±3.6	1.595
0.1193	6.97	28.80±0.01	224.6±3.4	1.584
0.1292	9.08	28.92±0.01	242.9±3.5	1.565
0.1481	14.1	29.15±0.01	316.8±3.9	1.527

NOTE.—Both the radio luminosities and flux densities have been corrected for the snapshot-bias (see text). The star-formation rate is taken from Brinchmann et al. (2004)

TABLE 2
RESULTS FOR $D_n(4000)$ BINNING

$D_n(4000)$	$z_{\rm median}$	$z_{\rm mean}$	$\log(L_{\rm radio,flux})$ [ergs/s/Hz]	$\log(L_{\rm radio,lum})$ [ergs/s/Hz]	$\log(L_{[\rm OIII]}/L_\odot)$	$\log(L_{[\rm OII]}/L_\odot)$
2.044	0.0724	0.0818	28.15	28.05	6.08	6.50
1.942	0.0826	0.0927	28.21	28.10	6.12	6.54
1.885	0.0873	0.0963	28.20	28.05	6.18	6.57
1.836	0.0928	0.0994	28.26	28.10	6.28	6.64
1.791	0.0951	0.1009	28.24	28.06	6.30	6.71
1.747	0.0960	0.1027	28.30	28.14	6.39	6.79
1.705	0.0972	0.1034	28.36	28.21	6.53	6.91
1.665	0.1008	0.1063	28.42	28.28	6.65	7.01
1.624	0.1014	0.1077	28.48	28.35	6.79	7.17
1.584	0.1031	0.1079	28.56	28.44	6.92	7.30
1.541	0.1053	0.1095	28.66	28.55	7.04	7.39
1.496	0.1069	0.1106	28.73	28.62	7.17	7.53
1.446	0.1114	0.1147	28.86	28.79	7.34	7.69
1.384	0.1143	0.1178	28.99	28.94	7.54	7.86
1.276	0.1201	0.1244	29.21	29.19	7.85	8.11

NOTE.—$\log(L_{\rm radio,flux})$ and $\log(L_{\rm radio,lum})$ are luminosities based on flux-stacking and luminosity-stacking, respectively. The bolometric luminosity of the sun ($L_\odot$) is 3.826×10^{33} ergs s^{-1}.

TABLE 3
INFERRED STAR-FORMATION RATES – STAR-FORMATION SUBSAMPLE

$z_{\rm median}$	$\log(L_{\rm radio})$ [ergs/s/Hz]	SFR [$M_\odot$ / yr]
0.075	27.60	0.45
0.095	28.10	1.07
0.100	28.34	1.61
0.101	28.46	1.97
0.106	28.57	2.37
0.108	28.72	3.06
0.112	28.78	3.38
0.115	28.91	4.49
0.119	28.99	5.40
0.123	29.08	6.64
0.128	29.23	9.38
0.134	29.34	12.1
0.149	29.65	24.7

NOTE.—For reference, an L_* galaxy corresponds to $\log(L_{\rm radio}) \approx 28.81$ and an SFR of 3.57 $M_\odot$ / year.